J_ID: z3w Customer A_ID: CYTO22518 Cadmus Art: CYTO22518 Ed. Ref. No.: 14-065 Date: 28-July-14 Stage: Page: 1

Cytometry PART A
Journal of the International Society for Advancement of Cytometry

Maximum Likelihood Estimation of FRET Efficiency and its Implications for Distortions in Pixelwise Calculation of FRET in Microscopy

Peter Nagy,[1*] Ágnes Szabó,[1,2] Tímea Váradi,[1] Tamás Kovács,[1] Gyula Batta,[1] János Szöllősi[1,2]

[1]Department of Biophysics and Cell Biology, University of Debrecen, Debrecen, Hungary

[2]MTA-DE Cell Biology and Signaling Research Group, University of Debrecen, Debrecen, Hungary.

Received 22 May 2014; Revised 4 July 2014; Accepted 18 July 2014

Grant sponsor: Hungarian Scientific Research Fund, Grant numbers: K103906, NK101337. Grant sponsor: European Union and the European Social Fund; TÁMOP-4.2.2.A-11/1/KONV-2012-0025.

*Correspondence to: Peter Nagy; Department of Biophysics and Cell Biology, University of Debrecen, Debrecen, Hungary. E-mail: szollo@med.unideb.hu

Published online 00 Month 2014 in Wiley Online Library (wileyonlinelibrary.com)

DOI: 10.1002/cyto.a.22518

Abstract

Ratiometric determination of the efficiency of fluorescence or Förster resonance energy transfer (FRET) is one of the most widespread methods for the characterization of protein clustering and conformation. Low photon numbers, often present in pixel-by-pixel determination of FRET efficiency in digital microscopy, result in large uncertainties in the derived FRET parameter. Here, we propose a method based on maximum likelihood estimation (MLE) of FRET efficiency using photon counting detectors to overcome this limitation. Intensities measured in the donor, FRET, and acceptor channels were all assumed to follow Poisson statistics as a result of detector shot noise. The joint probability of photon numbers detected in the donor, FRET, and acceptor channels was derived using an equation describing the relationship between the three measured intensities. The FRET efficiency generating the measured photon numbers with the largest likelihood was determined iteratively providing a single FRET value for all pixels in the calculation. Since as few as 100 pixels are sufficient to provide a maximum likelihood estimate for FRET, biological variability in FRET values can be revealed by performing the analysis for regions of interests in an image. Since the algorithm provides the probability of a combination of donor, FRET, and acceptor intensities observed in each individual pixel given a certain FRET efficiency, outlier pixels with low probabilities could be excluded from the analysis. Simulations carried out with low photon numbers in the presence and absence of outlier pixels revealed that the proposed approach can reliably and reproducibly estimate FRET efficiency. In addition, systematic evaluation of the simulation results showed that the distribution of pixel-by-pixel FRET efficiencies is skewed, and the mean of these FRET values is a biased and unreliable estimate of the FRET efficiency. In the absence of outlier pixels, FRET calculated from summed donor, FRET, and acceptor intensities proved to be as reliable as MLE. We conclude that MLE of FRET outperforms calculations using summed and pixel-by-pixel intensities in biologically relevant situations involving low photon numbers and outlier pixels. © 2014 International Society for Advancement of Cytometry

Key terms

FRET; maximum likelihood estimation (MLE); microscopy; Poisson statistics; error propagation

Introduction

Fluorescence or Förster resonance energy transfer (FRET) is regularly applied for analyzing the clustering and conformation of proteins (1–3). The radiationless transfer of energy from an excited donor to a nearby acceptor is manifested in several measurable changes, which has led to a multitude of different methods for calculating FRET. There are approaches measuring properties of either the donor or the acceptor including FRET-induced shortening of the donor lifetime, slowing of donor

ISAC International Society for Advancement of Cytometry

ID: kandasamy.d Time: 13:53 I Path: N:/3b2/CYTO/Vol00000/140078/APPFile/JW-CYTO140078

photobleaching, comparing donor intensities before and after acceptor photobleaching or saturation, comparing acceptor photobleaching in the presence and absence of the donor or measuring emission anisotropy to reveal homo- or hetero-FRET (1,4–10). Although these methods have been regularly used and have solid foundations, ratiometric or intensity-based approaches probably enjoy the most widespread use due to their affordability and flexibility.

Two different implementations of ratiometric measurement of FRET have been described: (i) the "three-cube" approach measuring intensities in three fluorescence channels corresponding to donor and acceptor fluorescence and FRET (2,11); (ii) spectral FRET measuring the emission spectrum (12,13). In a FRET system considered with full complexity there are five different species: (i) uncomplexed (acceptor-free) donor and acceptor-bound donor having emission characteristics of the donor and (ii) uncomplexed (donor-free) acceptor and donor-bound acceptor excited directly or by FRET having emission characteristics of the acceptor. Although uncomplexed donor and acceptor can be resolved under certain conditions, they are usually not considered leaving us with three species (12,13).

The literature abounds with FRET indices resulting from a somewhat arbitrary normalization of intensity measured in the FRET channel (14–16). No matter how enticing these methods are due to their simplicity, they have been shown to be nonlinear with respect to changes in FRET efficiency, and their quantitative correlation with the physical process of FRET and with the conformation or clustering of biomolecules is unclear (17). Therefore, quantitative determination of FRET efficiency is preferred, although k_t/k_f imaging (k_t and k_f are the rate constants of FRET and fluorescence decay, respectively) has been suggested to outperform the former approach due to its independence from the donor quantum yield and its superior properties at high FRET efficiencies (1,18).

Ratiometric measurement of FRET requires correction for spectral overspill and the determination of a factor variably called α or G expressing the fluorescence intensity ratio of an excited acceptor molecule detected in the FRET channel and an excited donor molecule measured in the donor channel (2,11,15,19). Determination of α is challenging, and several methods have been put forward for its determination (20–24). Complications can also arise in the measurement of spectral overspill factors due to their reported intensity dependence (25). Quantitative, ratiometric FRET measurements can be performed in fluorometry, flow cytometry and microscopy. The latter approach can reveal spatial heterogeneity in single cells; therefore, FRET is often calculated on a pixel-by-pixel basis. In such measurements photobleaching poses problems, which can be corrected (26) or exploited for resolving protein oligomerization states (27,28). Due to the low expression level of proteins and short pixel dwell times limited by phototoxicity and photobleaching the number of detected photons/pixel is often low. Consequently, large relative errors in the number of detected photons arise as a result of the Poissonian nature of photon statistics leading to large variance and systematic deviation in the calculated FRET efficiency due to error propagation. The effect and significance of this phenomenon have not been explored yet.

Here, we propose a method based on maximum likelihood estimation (MLE) of FRET efficiency to overcome the limitations posed by low photon numbers. Not only can our approach provide accurate estimates for the efficiency of FRET at low photon numbers, but it can also eliminate outlier pixels if their likelihood is low. Simulations of ratiometric FRET measurements with low photon numbers revealed significant distortions in pixel-by-pixel calculations of FRET efficiency. Evaluation of experimental and simulated data provides evidence that the proposed MLE of FRET efficiency is a reliable method for the estimation of FRET efficiency.

Theory

Basic Assumptions

In ratiometric measurement of FRET in microscopy intensities are measured in the donor, FRET and acceptor channels. If FRET is calculated on a pixel-by-pixel basis, spatial resolution comes at the price of low intensities resulting in large error in the FRET calculation (2). If intensities are averaged or summed in the image, error in the calculated FRET efficiency will be significantly reduced, but spatial resolution will be lost preventing us from excluding outlier pixels, that is, pixels in which the FRET efficiency is largely different from the rest of the image due to biological variation or measurement error other than photon statistics. In the current article we propose a method, which (i) reduces uncertainty in the calculated FRET efficiency introduced by error propagation in the presence of low photon numbers; (ii) is able to eliminate outlier pixels from the image. It is assumed that all pixels excluding the outliers can be characterized by a single FRET efficiency, which is calculated by MLE capitalizing on the Poisson statistics of photon detection. Therefore, a microscope equipped with photon counting detectors is required for the applicability of the method. Although the assumption of a single FRET efficiency for all pixels (i.e. the elimination of outlier pixels) overlooks biological variation, the uncertainty of pixel-wise FRET efficiencies under conditions of low photon counts would blur differences between pixel-by-pixel FRET values anyway. Therefore, under these conditions the presence of outlier pixels can most likely be attributed to measurement artifacts, which are to be eliminated. Although complex methods including MLE and spectral imaging have already been applied for reconstructing FRET images (13,29,30), our aim was to develop a method suitable for the most widely used, three-cube version of intensity-based or ratiometric FRET experiments in which only three images of the same field are acquired (donor, FRET, and acceptor channels).

Likelihood of the Measured Intensities

Intensities measured in the donor, FRET and acceptor channels are designated by I_1, I_2, and I_3, respectively, and they can be expressed as a function of the unquenched donor intensity (I_D), the directly excited acceptor intensity (I_A) and the FRET efficiency as follows (see Supporting Information, Table S1 for a definition of variables in the "Theory" section):

$$\begin{aligned} I_1 &= I_D(1-\mathrm{FRET}) + I_A S_4 + I_D\ \mathrm{FRET}\ \alpha \frac{S_4}{S_2} \\ I_2 &= I_D(1-\mathrm{FRET}) S_1 + I_A S_2 + I_D\ \mathrm{FRET}\ \alpha \\ I_3 &= I_D(1-\mathrm{FRET}) S_3 + I_A + I_D\ \mathrm{FRET}\ \alpha \frac{S_3}{S_1} \end{aligned} \tag{1}$$

where $S_{1–4}$ are spectral overspill factors and α compares the intensity of an excited acceptor molecule detected in the FRET channel to that of an excited donor molecule detected in the donor channel. S_1 and S_3 are the overspill of the donor to the FRET and acceptor channels, respectively, whereas S_2 and S_4 are the overspill of the acceptor to the FRET and donor channels, respectively. Detailed definitions of α and spectral overspill factors as well as considerations leading to equation set 1 have been published elsewhere (2,11). I_2 can be expressed as a function of I_1 and I_3 from equation set 1:

$$\begin{aligned} I_2 = {} & I_1 \frac{S_2((\mathrm{FRET}-1)S_1(S_1-S_2\ S_3)+\alpha\ \mathrm{FRET}(S_2\ S_3-S_1))}{\alpha\ \mathrm{FRET}\ S_2\ S_3\ S_4-S_1(\alpha\ \mathrm{FRET}\ S_4+(\mathrm{FRET}-1)S_2(S_3\ S_4-1))} \\ & + I_3 \frac{S_1\ S_2(S_2-S_1\ S_4)(\mathrm{FRET}-1)}{\alpha\ \mathrm{FRET}\ S_2\ S_3\ S_4-S_1(\alpha\ \mathrm{FRET}\ S_4+(\mathrm{FRET}-1)S_2(S_3S_4-1))} \\ & = I_1 c_d + I_3 c_a. \end{aligned} \tag{2}$$

The likelihood of the measured intensities is calculated assuming the intensities follow a Poisson distribution:

$$P = \prod_{k=1}^{n} \left(\left[\frac{(I_{1p,k}\ c_d + I_{3p,k}\ c_a)^{I_{2,k}}}{I_{2,k}!} e^{-(I_{1p,k}c_d + I_{3p,k}c_a)} \right] \cdot \left[\frac{I_{1p,k}{}^{I_{1,k}}}{I_{1,k}!} e^{-I_{1p,k}} \right] \cdot \left[\frac{I_{3p,k}{}^{I_{3,k}}}{I_{3,k}!} e^{-I_{3p,k}} \right] \right), \tag{3}$$

where the expression in the first, second and third square brackets correspond to the likelihood of the measured I_2, I_1, and I_3 intensities, respectively. Subscript p designates predicted intensities, which will have to be determined. P is the likelihood of the measured intensities determined as the product of the likelihood of individual pixels k for all of the n pixels assuming a FRET efficiency of *FRET* present in the constants c_d and c_a. The log-likelihood of the measured intensities is shown by the following equation:

$$\begin{aligned} L = \ln(P) = {} & -\sum_{k=1}^{n} \ln(I_{3,k}!) - \sum_{k=1}^{n} \ln(I_{1,k}!) - \sum_{k=1}^{n} \ln(I_{2,k}!) \\ & + \sum_{k=1}^{n} \ln(I_{3p,k}) I_{3,k} - \sum_{k=1}^{n} I_{3p,k} - c_a \sum_{k=1}^{n} I_{3p,k} \\ & + \sum_{k=1}^{n} \ln(I_{1p,k}) I_{1,k} - \sum_{k=1}^{n} I_{1p,k} - c_d \sum_{k=1}^{n} I_{1p,k} + \sum_{k=1}^{n} \ln(c_a I_{3p,k} + c_d I_{1p,k}) I_{2,k} \end{aligned} \tag{4}$$

Determination of the Predicted Intensities $I_{1,p}$ and I_{3p}

The partial derivatives of the log-likelihood function with respect to $I_{1p,k}$ and $I_{3p,k}$ are

$$\begin{aligned} \frac{\partial L}{\partial I_{1p,k}} &= \frac{I_{1,k}}{I_{1p,k}} - 1 - c_d + \frac{c_d I_{2,k}}{c_a I_{3p,k} + c_d I_{1p,k}}, \\ \frac{\partial L}{\partial I_{3p,k}} &= \frac{I_{3,k}}{I_{3p,k}} - 1 - c_a + \frac{c_a I_{2,k}}{c_a I_{3p,k} + c_d I_{1p,k}}. \end{aligned} \tag{5}$$

The predicted intensities maximize the log-likelihood; therefore, the zero of the partial derivatives is determined:

$$\frac{\partial L}{\partial I_{1p,k}} = 0, \quad \frac{\partial L}{\partial I_{3p,k}} = 0. \tag{6}$$

The meaningful, positive roots of the above quadratic equation set are

$$\begin{aligned} I_{1p,k} = {} & -\frac{1}{2(c_a-c_d)(1+c_d)} (c_d(I_{1,k}+I_{2,k}) - c_a((1+c_d)I_{3,k} + (2+c_d)I_{1,k} + I_{2,k}) + \\ & + \sqrt{-4c_a(c_a-c_d)(1+c_d)I_{1,k}(I_{1,k}+I_{2,k}+I_{3,k}) + (c_d(I_{1,k}+I_{2,k}) - c_a((1+c_d)I_{3,k} + (2+c_d)I_{1,k} + I_{2,k}))^2}) \\ I_{3p,k} = {} & \frac{1}{2(c_a-c_d)(1+c_a)} (c_a(I_{3,k}+I_{2,k}) - c_d((1+c_a)I_{1,k} + (2+c_a)I_{3,k} + I_{2,k}) + \\ & + \sqrt{-4c_a(c_a-c_d)(1+c_d)I_{1,k}(I_{1,k}+I_{2,k}+I_{3,k}) + (c_d(I_{1,k}+I_{2,k}) - c_a((1+c_d)I_{3,k} + (2+c_d)I_{1,k} + I_{2,k}))^2}). \end{aligned} \tag{7}$$

Determination of the FRET Efficiency

Parameters c_d and c_a defined in Eq. (2) and the predicted I_1 and I_3 intensities calculated according to Eq. (7) were substituted into Eq. (4). The only free parameter remaining in the above expression is the FRET efficiency. The FRET value at which the above expression reached its maximum was considered to be the maximum likelihood estimate of FRET. Since the maximum likelihood function is strictly unimodal, that is, it does not have local extrema, its local maximum was found by the FindMaximum function of Mathematica (Wolfram Research, Champaign, IL). The confidence interval of the determined FRET efficiency was determined by plotting the likelihood of the measured intensities as a function of the FRET efficiency.

Discrimination of Outlier Pixels using Thresholded Maximum Likelihood Estimation: Threshold MLE

Equations (3) and (4) give the likelihood of each pixel. Even when all pixels are characterized by a single FRET

efficiency without significant biological variation or measurement error other than photon statistics (i.e. no outlier pixels present), there will be a distribution of likelihood values. A threshold likelihood is chosen based on such a simulated dataset without outlier pixels corresponding to the 10th percentile or other arbitrarily chosen percentile of the likelihood distribution. When analyzing the dataset containing outlier pixels only pixels whose likelihood is higher than the threshold will be included in calculating the overall likelihood of all pixels in the image, that is, the summation in Eq. (4) or the product in Eq. (3) will only include pixels above the threshold likelihood. As shown in the results section this approach efficiently eliminates outlier pixels from the measured data set.

Maximum Likelihood Estimation of Spectral Overspill Factors

The procedures outlined in the preceding sections can also be used for estimating spectral overspill factors (S_{1-4}) in Eqs. (1), (2). The relationship between two intensities (I_x, I_y) is described by the following linear equation:

$$I_y = S\ I_x + b \tag{8}$$

In this equation the proposed intensity dependence of overspill factors is disregarded (25). Indeed, we will show in the results section that the Poisson statistics of photon detection can lead to the observed intensity dependence in ratio parameters. The likelihood of the measured intensities is

$$P=\prod_{k=1}^{n}\left(\left[\frac{\left(S\ I_{xp,k}+b\right)^{I_{y,k}}}{I_{y,k}!}e^{-\left(S\ I_{xp,k}+b\right)}\right]\left[\frac{{I_{xp,k}}^{I_{x,k}}}{I_{x,k}!}e^{-I_{xp,k}}\right]\right), \tag{9}$$

where the expressions in the 1st and 2nd square brackets correspond to the likelihood of I_y and I_x, respectively. The log-likelihood is expressed by the following equation:

$$\begin{aligned} L=\ln(P)=&-b\ n-\sum_{k=1}^{n}\ln\left(I_{x,k}!\right)-\sum_{k=1}^{n}\ln\left(I_{y,k}!\right)\\ &+\sum_{k=1}^{n}\ln\left(I_{xp,k}\right)I_{x,k}-\sum_{k=1}^{n}I_{xp,k}-\\ &-S\sum_{k=1}^{n}I_{xp,k}+\sum_{k=1}^{n}\ln\left(b+S\ I_{xp,k}\right)I_{y,k}, \end{aligned} \tag{10}$$

with $I_{xp,k}$ standing for predicted intensities of I_x. The predicted intensities are determined by equating the partial derivative of the log-likelihood with respect to $I_{xp,k}$ to zero:

$$\frac{\partial L}{\partial I_{xp,k}}=\frac{S\ I_{y,k}}{S\ I_{xp,k}+b}-S+\frac{I_{x,k}}{I_{xp,k}}-1=0. \tag{11}$$

The meaningful, positive root of the above quadratic equation is

$$I_{xp,k}=\frac{-b(1+S)+S\left(I_{x,k}+I_{y,k}\right)+\sqrt{4bS(1+S)I_{x,k}+\left(b(1+S)-S\left(I_{x,k}+I_{y,k}\right)\right)^2}}{2S(1+S)}. \tag{12}$$

We can proceed in two different ways to derive S and b in Eq. (8). In the first approach the partial derivatives of the log-likelihood with respect to S and b are determined:

$$\begin{aligned} \frac{\partial L}{\partial S}&=-\sum_{k=1}^{n}I_{xp,k}+\sum_{k=1}^{n}\frac{I_{y,k}\ I_{xp,k}}{b+S\ I_{xp,k}}=\sum_{k=1}^{n}\left(I_{xp,k}\left(\frac{I_{y,k}}{b+S\ I_{xp,k}}-1\right)\right)\\ \frac{\partial L}{\partial b}&=-n+\sum_{k=1}^{n}\frac{I_{y,k}}{b+S\ I_{xp,k}}=\sum_{k=1}^{n}\left(\frac{I_{y,k}}{b+S\ I_{xp,k}}-1\right). \end{aligned} \tag{13}$$

Solving equation set 13 after substituting Eq. (12) yields the overspill factor S and the intercept b. In most cases the intercept can be assumed to be zero significantly simplifying the equation for $I_{xp,k}$:

$$I_{xp,k}=\frac{I_{x,k}+I_{y,k}}{1+S}. \tag{14}$$

Substituting Eq. (14) into Eq. (13) yields

$$\frac{\partial L}{\partial S}=\sum_{k=1}^{n}\left(\frac{I_{x,k}+I_{y,k}}{1+S}\left(\frac{I_{y,k}}{S\ \frac{I_{x,k}+I_{y,k}}{1+S}}-1\right)\right). \tag{15}$$

Equating the above equation with zero and numerically solving for S provides the spectral overspill factor assuming a zero intercept.

In the second approach Eq. (12) is substituted into Eq. (10) and the maximum of the log-likelihood is found by varying S and b, or only S if the intercept is assumed to be zero using Mathematica. The second approach is preferred since it yields the likelihood of each pixel providing for the elimination of outlier pixels with likelihood values under the threshold.

Materials and Methods

Simulations

Monte Carlo simulations were carried out to test whether the approach outlined in the Theory section can be applied to estimate FRET. Four different simulations were carried out in Mathematica:

A. Determination of FRET efficiency in the absence of outlier pixels: The unquenched donor (I_d) and directly excited acceptor (I_a) intensities were assumed to follow a normal distribution with parameters described in Table 1. Three different intensity ranges were tested with photon numbers as low as 5 photons/pixel. I_1–I_3 expected intensities were calculated according to Eq. (1) using overspill factors and the α parameter shown in Table 1. The detected photon numbers in the I_1–I_3 channels were generated according to the Poisson distribution using the I_1–I_3 expected T1

J_ID: z3w Customer A_ID: CYTO22518 Cadmus Art: CYTO22518 Ed. Ref. No.: 14-065 Date: 28-July-14 Stage: Page: 5

intensities as mean values. FRET was determined by MLE, on a pixel-by-pixel basis and from summed intensities as described elsewhere (2,11,22).

B. Determination of FRET efficiency in the presence of outlier pixels (thresholded MLE): A random dataset of 10000 pixels was generated according to parameters of the medium intensity condition (mean photon number of 10 for I_d and I_a) specified in Table 1. FRET was estimated using the maximum likelihood approach and the likelihood of each pixel at the estimated FRET value was calculated according to Eq. (3). The 10th percentile of the likelihood distribution was chosen as the threshold value. Next, the dataset was contaminated by adding a Gaussian noise with mean values of 10, 5 and 15 in the I_1, I_2 and I_3 channels, respectively, to 1/3 of the pixels. FRET was evaluated using the thresholded MLE approach using the cutoff likelihood determined as described above.
C. Determination of overspill factors in the absence of outlier pixels: Intensity *FL-X* was assumed to spill over to intensity *FL-Y*. A normally distributed random dataset was generated ($\mu=10$, $\sigma=10$) and the overspill factor was assumed to be 0.25, i.e. $FL\text{-}Y=0.25\cdot FL\text{-}X$. Poissonian noise was added to both *FL-X* and *FL-Y* to simulate a microscope working in the photon counting mode. The simulated *FL-X* and *FL-Y* intensities were used for determining the overspill factor.
D. Determination of overspill factors in the presence of outlier pixels (thresholded MLE): A random dataset with parameters in point iii was generated and the overspill factor was determined using MLE. The likelihood of every pixel at the determined overspill factor was calculated according to Eq. (9), and the (10)th percentile of the likelihood distribution was chosen as the threshold likelihood. A Gaussian noise with a mean and SD of 20 and 25, respectively, was added to both channels in every second pixel and the overspill factor was evaluated with the thresholded MLE method using the threshold likelihood determined as described above.

Table 1. Parameters for generating a FRET dataset used for simulation of the MLE process

	LOW	MEDIUM	HIGH
FRET		0.25	
S_1		0.3	
S_2		0.4	
S_3		0.05	
S_4		0.02	
α		0.05	
I_d (photon number, mean $\pm$ SD)	5 ± 1	10 ± 2	25 ± 5
I_a (photon number, mean $\pm$ SD)	5 ± 1	10 ± 2	25 ± 5

Five-thousand normally distributed random numbers corresponding to the unquenched donor (I_d) and directly excited acceptor intensities (I_a) were generated according to the mean and SD parameters shown in the table. The expected values of I_1–I_3 intensities were calculated according to Eq. (1) using the parameters in the table. Three different data sets were created with low, medium and high photon numbers with identical spectroscopic constants and FRET value. The measured intensities were generated by a Poisson process using the expected I_1–I_3 intensities as mean values of the Poisson distribution.

Confocal Microscopy

Image acquisition was carried out on an Olympus FV1000 confocal microscope run in pseudo-photon counting mode using a 60× oil immersion objective (N.A.= 1.35). In pseudo-photon counting mode the pixel dwell time is split into smaller time windows for which the analog output of the photomultiplier tube (PMT) has been calibrated with respect to photon numbers. However, the final integrated, digital readout parameter of the PMT is not equal to the absolute photon count, but the photon number multiplied by a constant, which had to be determined as described elsewhere (31). In the experiment with fluorescent proteins excitation in the donor (Cerulean) and FRET channels was performed at 458 nm, and emission was detected in the wavelength range of 475–505 and 530–630 nm, respectively. The acceptor (Venus) was excited at 515 nm and detected between 530 and 630 nm. For imaging antibody-stained tissue samples the donor (AlexaFluor546) was excited at 543 nm and its emission was measured between 555 and 625 nm. The acceptor (AlexaFluor647) was excited at 633 nm and detected between 655 and 755 nm. Images corresponding to the FRET channel were recorded using the excitation wavelength of the donor and the emission range of the acceptor. Measurement of emission in spectral ranges was carried out with the spectral detectors of the microscope. The pixel dwell time was varied between 2 and 10 μs.

Calculation of FRET Efficiency

Images stored as TIFF files were processed using the DipImage toolbox (University of Technology, Delft, The Netherlands) in Matlab (Mathworks, Natick, MA). Each channel was background-corrected by subtracting a constant corresponding to the intensity of a label-free area from every pixel. The images were thresholded, and the intensity values of pixels above the threshold were exported to Mathematica where all further analysis was carried out. Calculation of FRET efficiency on a pixel-by-pixel basis and from summed intensities was performed using a formalism described previously (2). MLE of FRET was carried out as described in the Theory section.

Cells, Tissue Samples, Plasmids and Antibodies

HeLa cells obtained from ATCC (American Type Culture Collection, Manassas, VA) were cultured according to their specifications. Cells plated in 8-well chambered coverglasses (Planegg, Germany) were transfected with plasmids encoding Cerulean, Venus, C5V, C17V, and C32V (32) constructs 2 days before confocal microscopy. The plasmids code for soluble fluorescent proteins used as donor (Cerulean), acceptor (Venus), and FRET (C5V, C17V, C32V) standards. The FRET calibration constructs contain donor and acceptor separated by amino acid linkers of different lengths (32). Transfection was carried out using 0.3 μg DNA/well by Lipofectamine2000

ID: kandasamy.d Time: 13:54 I Path: N:/3b2/CYTO/Vol00000/140078/APPFile/JW-CYTO140078

Table 2. Results of MLE of FRET using the simulated data set shown in Table 11

		LOW	MEDIUM	HIGH
MLE		0.23 ± 0.01	0.24 ± 0.01	0.25 ± 0.01
Pixelwise FRET	Mean	1.16 ± 0.08	0.09 ± 0.14	0.16 ± 0.2
	Trimmed mean	0.48 ± 0.03	0.19 ± 0.02	0.16 ± 0.01
	Median	0.5 ± 0.01	0.34 ± 0.01	0.25 ± 0.01
FRET from summed intensities		0.21 ± 0.01	0.24 ± 0.01	0.25 ± 0.01

Random, measured intensities were generated according to Table 1 assuming a FRET = 0.25. The process was repeated 100-times and the FRET efficiency was estimated by five different methods for each dataset consisting of 5,000 I_1–I_3 data triplets. The mean±SD of the calculated FRET values are shown in the table.

(Life Technologies/Thermo Fisher Scientific, Waltham, MA). The Lipofectamine2000/DNA ratio was 1:0.3.

Tissue samples of breast cancer patients were obtained from the Uzsoki Teaching Hospital (Budapest, Hungary) and they were stored in liquid nitrogen. A total of 4 μm sections were cut with a cryostat and tissue slices were stored at −70°C until staining. Samples were fixed in 4% HCHO for 30 min on ice followed by blocking in 1% BSA for another 30 min. Cells were labeled with 20 μg/mL AlexaFluor546-trastuzumab and/or AlexaFluor647-pertuzumab at 4°C overnight followed by washing and covering with Mowiol (Sigma-Aldrich, St. Louis, MO). Trastuzumab and pertuzumab are humanized monoclonal antibodies against two non-overlapping epitopes of ErbB2. When one of the antibodies is labeled with a donor, while the other with a suitable acceptor, they constitute an intramolecular FRET pair due to the fact that the antibodies do not compete with each other, but they are sufficiently close to each other for FRET to take place (33). Trastuzumab was purchased from Roche (Basel, Switzerland) while pertuzumab was a kind gift from Genentech (South San Francisco, CA). Antibodies were labeled with AlexaFluor dyes (Life Technologies/Thermo Fisher Scientific) according to the specifications of the manufacturer. Collection of patient material has been approved by the Science and Research Ethics Committee of the National Health Science Council of Hungary (ad.335/PI/2007). Informed consent has been obtained from all patients by the physicians responsible for their treatment.

Results and Discussion

Maximum Likelihood Estimation of FRET Efficiency in the Absence of Outlier Pixels

Monte Carlo simulations with parameters described in the Methods section were carried out to evaluate the method based on MLE for FRET measurements. In a single simulation a dataset of 5000 pixels was generated and FRET was determined using five different approaches: (i) MLE; (ii–iv) the mean, trimmed mean and median of FRET efficiencies calculated on a pixel-by-pixel basis; and (v) FRET calculated from summed I_1–I_3 intensities. In order to test the reliability of the different approaches the simulation was repeated 100-times. MLE of FRET reproducibly estimated the FRET efficiency of 0.25 used in the simulations even under conditions of extremely low photon numbers judged from the SD values (Table 2). FRET calculated from summed intensities was as reliable as MLE, while pixelwise calculation turned out to be a poor estimate of the simulated FRET efficiency since only the median at relatively high photon numbers (25 photons/pixel) was accurate and precise. (The term accuracy describes how close the estimate is to the simulated value and it is judged by the mean. Precision or reproducibility is related to how close repeated estimations are to the simulated FRET values and it is evaluated from the SD values.) The poor performance of pixelwise FRET calculations at low photon numbers is also exemplified by the wide distribution of FRET efficiencies in a single Monte Carlo simulation (Fig. 1). Although the low and medium intensity datasets probably represent extreme conditions, FRET histograms similar to that in Figure 1C (high intensity dataset) are not uncommon in FRET microscopy (34). Since a single FRET efficiency was assumed for all pixels in the simulations, the shape of the histograms is solely determined by error propagation, and it has nothing to do with any pixel-by-pixel heterogeneity in the FRET efficiency. This finding supports the assumption that a single FRET value is sufficient to describe the distribution of calculated FRET efficiencies under conditions of low intensity. The confidence interval of MLE was determined by calculating the likelihood of the simulated intensities according to Eq. (3) as a function of FRET efficiency. The confidence plots also reveal that MLE provides an excellent estimate for the simulated FRET value (Fig. 1). All these analyses convincingly show that the maximum likelihood approach and calculations using summed intensities are accurate and precise estimators of FRET. By comparing different estimators of ratio parameters (e.g. overspill factors) calculations from summed intensities have also been found to perform significantly better than those using pixel-by-pixel intensities (35).

Standard Deviation and Confidence Interval of Maximum Likelihood Estimation of FRET as a Function of the Number of Pixels

MLE turned out to be a suitable method to determine FRET efficiency, but it sacrifices the ability to uncover pixel-by-pixel differences since a single estimate is provided for all the pixels in the dataset. However, it is possible to analyze regions of interest separately in an image using MLE to reveal spatial heterogeneity. Therefore, it is of importance to determine how the size of the dataset determines the reliability and

J_ID: z3w Customer A_ID: CYTO22518 Cadmus Art: CYTO22518 Ed. Ref. No.: 14-065 Date: 28-July-14 Stage: Page: 7

COLOR

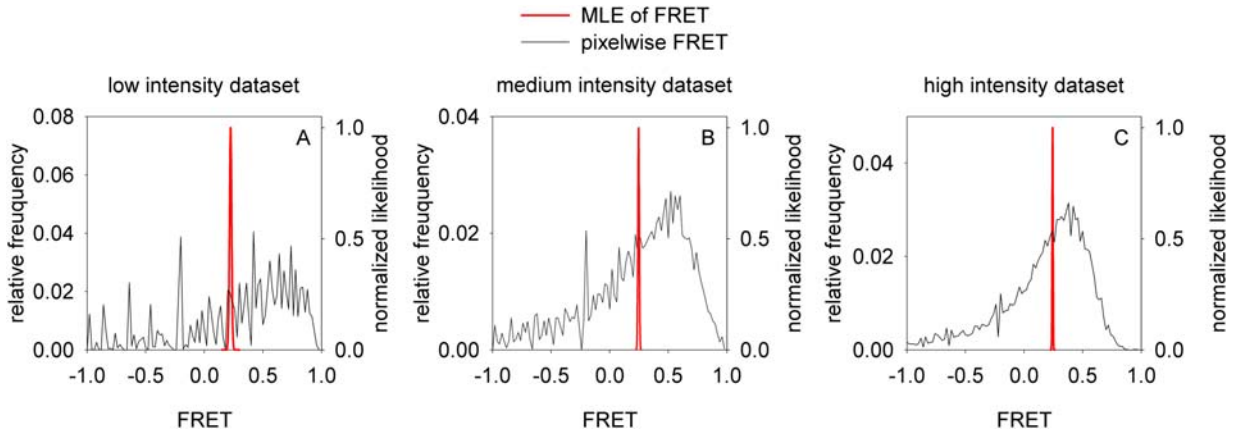

Figure 1. Maximum likelihood estimation and pixelwise calculation of FRET efficiency with simulated datasets. Datasets containing 5000 pixels were generated according to Table 1 with a simulated FRET value of 0.25. The distribution of FRET values calculated on a pixel-by-pixel basis is shown by the thin black lines. FRET was also determined by MLE and the normalized likelihood values display the confidence plot (thick red lines).

reproducibility of the approach. The simulation using the medium intensity dataset described in the previous section was carried out 100-times with datasets of different sizes ranging from 12 to 6400 pixels. The results showed that as few as 100–200 pixels were sufficient to provide reasonably accurate and precise estimates for the simulated FRET value (Fig. 2). The confidence plots of single MLE estimations also confirmed this conclusion. A dataset of 100 pixels may be derived from a square region of interest with a width of 10 pixels corresponding to a distance of 1 μm assuming a pixel size of 100 nm. Therefore, these simulations show that subcellular resolution can be achieved by MLE with intensities as low as 10 photons/pixel. Consequently, cells or regions of interest inside cells can be analyzed separately to reveal biological variation. It has to be noted that the spatial resolution of ~1 μm described above translates to true resolution only if the pixel size of the microscope matches its optical resolving power according to the Nyquist criterion. Determination of spatially resolved FRET efficiency is further discussed in the Supporting Information ("Spatial resolution achieved in MLE of FRET efficiency").

Maximum Likelihood Estimation of FRET Efficiency in the Presence of Outlier Pixels: Thresholded MLE

There is another way of endowing MLE with the ability to resolve spatial heterogeneity. In many biological samples a subpopulation of pixels, designated outlier pixels, is contaminated by noise of biological or instrumental origin. While it is justified to remove pixels standing out of the majority of pixels as a results of instrumental noise, biologically relevant heterogeneity should not be overlooked. However, under conditions of low photon counts, where the MLE approach is advised to be used, biological heterogeneity is unlikely to be detected as a result of the wide distribution of the pixelwise FRET histograms as demonstrated previously (Fig. 1, Table 2). Therefore, pixels to be removed are assumed to result from noise of instrumental origin in the forthcoming discussion. If these pixels are included in the calculation, they will significantly distort the estimation. The maximum likelihood approach provides a way to eliminate these outlier pixels if MLE is performed only with pixels with likelihood values above a cutoff value (thresholded MLE). The threshold likelihood was determined from a simulated dataset of pixels without outlier values as described in the Methods section (Fig. 3A), and thresholded MLE was carried out with a dataset in which 1/3 of the pixels contained Gaussian noise (see the "Methods" section for details of the simulation). The analysis revealed that only the thresholded maximum likelihood approach was able to provide a precise and accurate estimate for the simulated FRET efficiency (Table 3). The likelihood distribution of all pixels revealed an extra peak below the likelihood threshold (Fig. 3B). Most of these pixels corresponded to the pixels with added Gaussian noise (Fig. 3C, Supporting Information, Fig. S2). The confidence plot of a single thresholded MLE and the distribution of FRET values resulting from repeating the estimation 100-times both confirm the reliability of the approach (Fig. 3D). It is important to point out that neither calculations with pixelwise, nor with summed intensities provided a good estimate for the simulated FRET efficiency. One may assume that the histogram of pixelwise FRET efficiencies or a dot plot of photon numbers provide a way to eliminate outlier pixels. However, the histogram of calculated pixelwise FRET intensities corresponding to pixels with and without added noise show a considerable overlap preventing us from recognizing outlier pixels (Fig. 3E). Similarly, the two dimensional histogram of detected intensities in the FRET and donor channels seems to contain a single population making the discrimination of outlier pixels impossible (Fig. 3F).

Maximum Likelihood Estimation of Spectral Overspill Factors

It has already been suggested that pixelwise calculations provide a biased estimate for overspill parameters (35). We compared the performance of MLE estimation and calculations using pixelwise and summed intensities to estimate

ID: kandasamy.d Time: 13:54 I Path: N:/3b2/CYTO/Vol00000/140078/APPFile/JW-CYTO140078

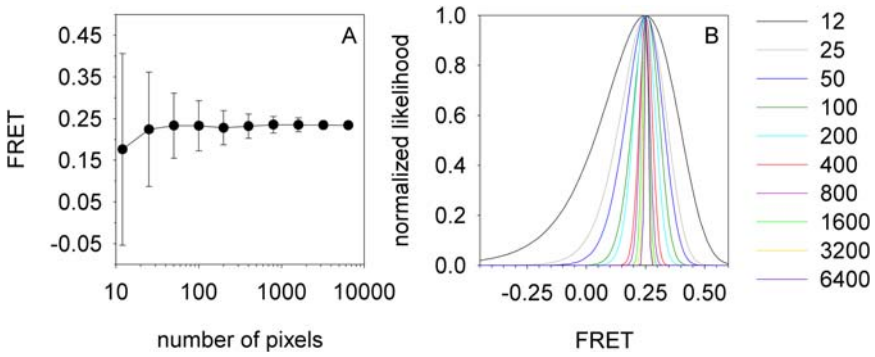

C
O
L
O
R

Figure 2. The number of pixels influences the uncertainty of maximum likelihood estimation of FRET. (**A**) Random datasets containing different number of pixels was generated using parameters of the medium intensity condition described in Table 1. The simulation was repeated 100-times and the mean ± SD of the FRET values determined by MLE are shown as function of the size of the dataset. (**B**) The confidence interval of a single MLE of FRET is plotted for datasets of different sizes. The number of pixels contained in the simulated dataset is shown in the legend.

AQ2

overspill parameters. Approaches based on MLE or those using summed intensities turned out to be equally reliable in the absence of outlier pixels (Supporting Information, Table S2). In light of the results described in the previous section outlier pixels were expected to bias the estimation using summed intensities significantly. In order to test this assumption a random data set, described in detail in the Supporting Information (Table S2 and Fig. S3), was generated. Using a cutoff likelihood determined from a dataset without outlier pixels thresholded MLE was carried out providing a reliable estimate for the simulated overspill parameter (Supporting Information,Table S3, Fig. S3). Conclusions reached from thresholded MLE of overspill parameters are similar to those described for thresholded MLE of FRET: (i) neither pixelwise calculations, nor calculations from summed intensities provided an accurate estimate for the simulated ratio parameter in the presence of outlier pixels (Supporting Information,Table S2). In addition, conventional linear regression also misestimated the overspill parameter (Supporting Information, Fig. S3F). (ii) Most outlier pixels were correctly identified by the algorithm because their likelihood was under the threshold (Supporting Information, Fig. S3C); (iii) Observation of histograms of the overspill parameter calculated on a pixel-by-pixel basis (Supporting Information, Fig. S3E) or dot plots of intensities (Supporting Information, Fig. S3F) did not reveal the outlier pixels.

Poisson Statistics of Photon Detection Leads to Intensity Dependence of Overspill Factors

Ratio or overspill parameters are important in many biological applications of image analysis. Therefore, considerable attention has been paid to their accurate and reproducible determination (25,35). Although it is usually assumed that the ratio of intensities of a fluorophore detected in two distinct wavelength ranges by two detectors is constant, intensity dependence of overspill parameters has recently been reported (25). Intensity dependent detector gain and spread of the signal to neighboring pixels have been blamed for this phenomenon (25,36). Here, we intend to show that such apparent intensity dependence of ratio parameters calculated on a pixel-by-pixel basis also arises as a result of the statistical nature of photon detection. Intensities distributed according to various distributions were generated (*FL-X*) followed by calculating the *FL-Y* intensity assuming that 25% of the *FL-X* intensity spills over to *FL-Y*. Poisson noise was added to both intensities and the overspill parameter was determined on a pixel-by-pixel basis. Depending on the distribution of the *FL-X* intensity various intensity dependencies were generated (Supporting Information, Fig. S4). The apparent intensity dependence was typically much more significant if the mean *FL-X* intensity was low (Supporting Information, Fig. S4B–D). There is a tendency to overestimate the overspill parameter at low intensities and to underestimate it at high intensities. This phenomenon is accounted for in the Supporting Information. Although any kind of noise is expected to distort the calculation of the ratio (overspill) parameter, the significance of our finding lies in the fact that detector shot noise is unavoidable and will therefore always be present in any kind of measurement in which the signal to noise ratio is low.

Maximum Likelihood Estimation of FRET Efficiency using Cerulean-Venus Constructs

Having established the theoretical foundation and applicability of MLE-based FRET evaluation on simulated datasets the method was tested on experimental data. Cells were transfected with fusion constructs of Cerulean and Venus in which the two fluorescent proteins were separated by linkers of different lengths (32). Spectroscopic overspill factors (S_{1-4}) were determined in cells transfected with only Cerulean or Venus using MLE (Supporting Information, Fig. S5). The α parameter was calculated using the Cerulean-Venus fusion constructs as described previously (Ref. [20), Supporting Information, Fig. S5). The images for FRET calculations were recorded in the photon counting mode of a confocal microscope using low laser intensities to ensure low photon numbers (~5–10 photons/pixel). MLE provided FRET values which were in agreement with published results (C5V: 0.42 ± 0.04; C35V: 0.3 ± 0.03 according to MLE (Fig. 4A) compared to published results obtained by fluorescence lifetime-based FRET

F4

J_ID: z3w Customer A_ID: CYTO22518 Cadmus Art: CYTO22518 Ed. Ref. No.: 14-065 Date: 28-July-14 Stage: Page: 9

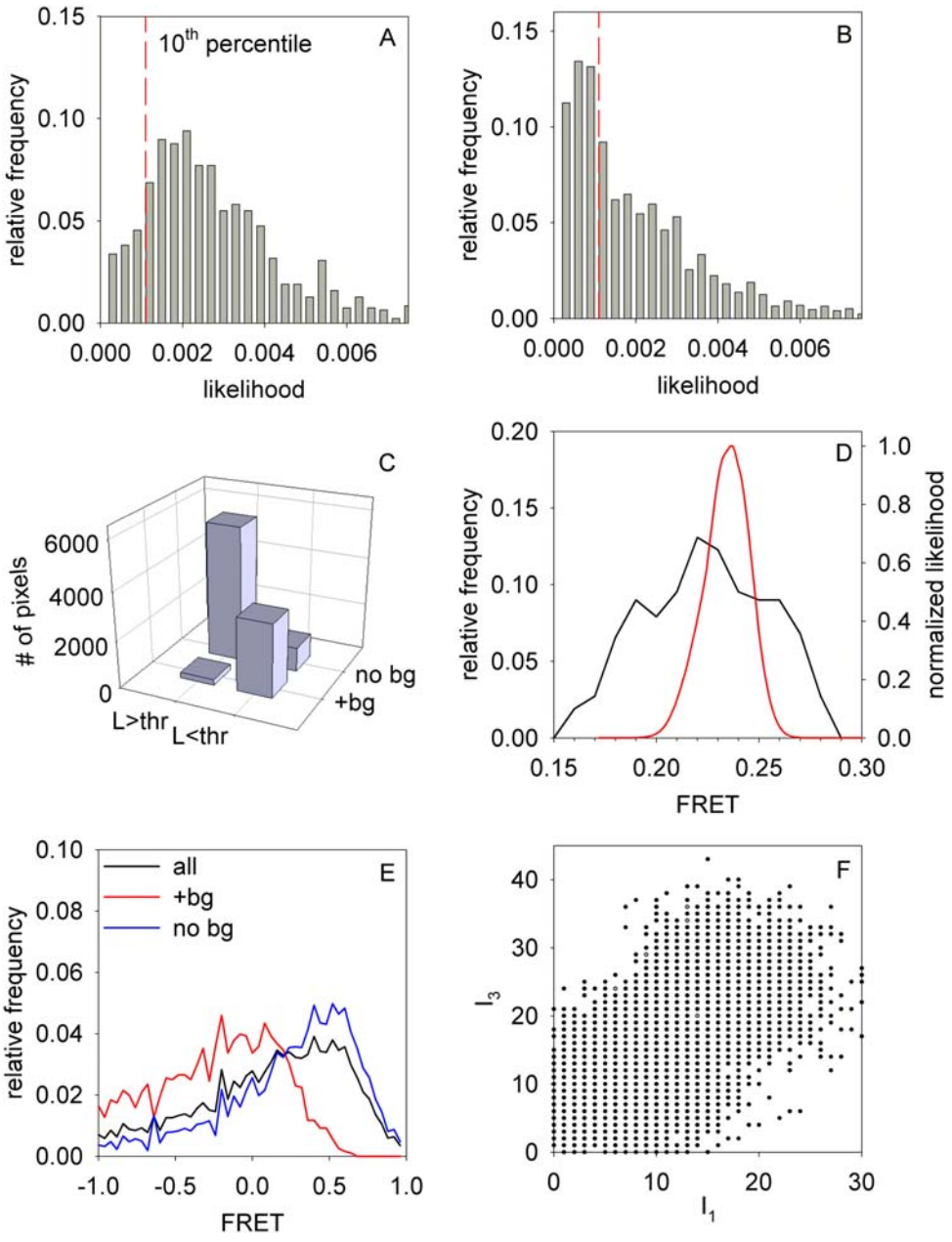

COLOR

Figure 3. Maximum likelihood estimation of FRET in the presence of outlier pixels. (**A**) A random dataset of 10,000 pixels was generated using parameters of the medium intensity condition described in Table 1. FRET was determined by MLE. The likelihood of individual pixels was calculated and their distribution was displayed. The likelihood corresponding to the 10th percentile is shown by the red dashed line. (**B**) A random dataset described in (A) was generated and Gaussian noise was added to 1/3 of the pixels (for details consult the Methods section). FRET was calculated by MLE using pixels whose likelihood was above the 10th percentile determined in (A) (thresholded MLE). The distribution of likelihood values of all pixels (both above and below the threshold) was plotted. The red dashed line shows the 10th percentile from A for comparison. (**C**) FRET was determined by thresholded MLE from the dataset described in (B). The number of pixels in which the likelihood was below (L<thr) and above (L>thr) the threshold (10th percentile in A) was determined for pixels with ("+bg") or without ("no bg") Gaussian noise showing that pixels with added Gaussian noise are more likely to be under the likelihood threshold than those without added noise. (**D**) The confidence plot of a single, thresholded MLE of FRET using the dataset containing outlier pixels [described in (B)] was calculated and shown as normalized likelihood values by the red line. The same simulation was repeated 100-times and the distribution of FRET efficiencies determined by thresholded MLE is shown (black line). (**E**) FRET was calculated on a pixel-by-pixel basis using the dataset described in B. The distribution of FRET values of all pixels ("all"), those with ("+bg") and without ("no bg") added Gaussian noise is shown. (**F**) Two-dimensional histogram of the simulated I_1 and I_3 intensities of the dataset described in (B).

measurements (32): 0.43 ± 0.02 (C5V), 0.31 ± 0.02 (C35V). $P > 0.6$ for the comparison of our and published results using Student's *t*-test.). On the other hand, pixelwise calculations were difficult to interpret. The FRET histogram was wide and asymmetrical giving the false impression of heterogeneity. From among measures of central tendency only the median

ID: kandasamy.d Time: 13:54 I Path: N:/3b2/CYTO/Vol00000/140078/APPFile/JW-CYTO140078

J_ID: z3w Customer A_ID: CYTO22518 Cadmus Art: CYTO22518 Ed. Ref. No.: 14-065 Date: 28-July-14 Stage: Page: 10

Table 3. Maximum likelihood estimation of FRET in a dataset containing outlier pixels

		ESTIMATED FRET
Thresholded MLE		0.22 ± 0.03
Pixelwise FRET	Mean	0.02 ± 0.75
	Trimmed mean	−0.01 ± 0.04
	Median	0.14 ± 0.03
FRET from summed intensities		−0.08 ± 0.03

Random, measured intensities of 10,000 pixels were generated according to the medium intensity dataset described in Table 1 and 1/3 of the pixels was contaminated with a Gaussian noise with mean values of 10, 5, 15 in the I_1, I_2, and I_3 channels, respectively. The simulation was repeated 100-times and FRET was estimated by five different approaches. The mean ± SD of the estimates is displayed in the table.

provided a reasonable estimate for the FRET efficiency (medians for the C5V and C35V constructs were 0.4 ± 0.05 and 0.31 ± 0.03, respectively). These findings were in agreement with those obtained in simulations. These findings have important implications for designing experiments. In many studies aimed at investigating protein interactions the targets fused to fluorescent proteins are expressed at a high level in order to have sufficiently high fluorescence intensities. But overexpression of proteins can lead to the generation of such interactions which are not present under physiological or even pathologically increased expression levels. The methods presented in the current article make reliable estimation of FRET efficiencies possible at significantly lower expression levels at which nonspecific interactions are not expected to form.

Maximum Likelihood Estimation of FRET Efficiency in Tissue Samples

MLE of FRET was tested on tissue samples, a challenging experimental condition due to high autofluorescence and the presence of outlier pixels. ErbB2-overexpressing breast cancer tissue samples were labeled with AlexaFluor546-trastuzumab and AlexaFluor647-pertuzumab constituting a FRET pair for measuring intramolecular energy transfer between two non-overlapping epitopes of ErbB2. MLE-based determinations of FRET in images without outlier pixels provided FRET values (0.34 ± 0.05) in agreement with previous results and with measurements carried out with SKBR-3 breast cancer cells labeled with the same kind of antibodies (0.3 ± 0.03, $P > 0.3$) (Ref. [33], Fig. 4B). Pixelwise calculation of FRET in the same samples performed reasonably well with the median providing the best estimate. The reason for the reliability of pixelwise calculations lies in the significantly higher photon number (∼20–30 photons/pixel) than in experiments with the Cerulean-Venus fusion constructs (∼5–10 photons/pixel).

The method was also evaluated on images with outlier pixels. Thresholded MLE provided a FRET value of 0.38 ± 0.05 by eliminating most outlier pixels from the analysis (Fig. 4C and Supporting Information, Fig. S6). These findings are in reasonably good agreement with results obtained for a sample without outlier pixels (see previous paragraph, $P > 0.3$). Calculations from summed and pixelwise intensities were also carried out, but all of these methods provided inaccurate estimates (FRET from summed intensities: 0.57 ± 0.04; median of pixelwise FRET: 0.52 ± 0.05). MLE without thresholding also misestimated the FRET value (0.57 ± 0.04). The reason for the failure of methods other than thresholded MLE becomes apparent when observing the distribution of

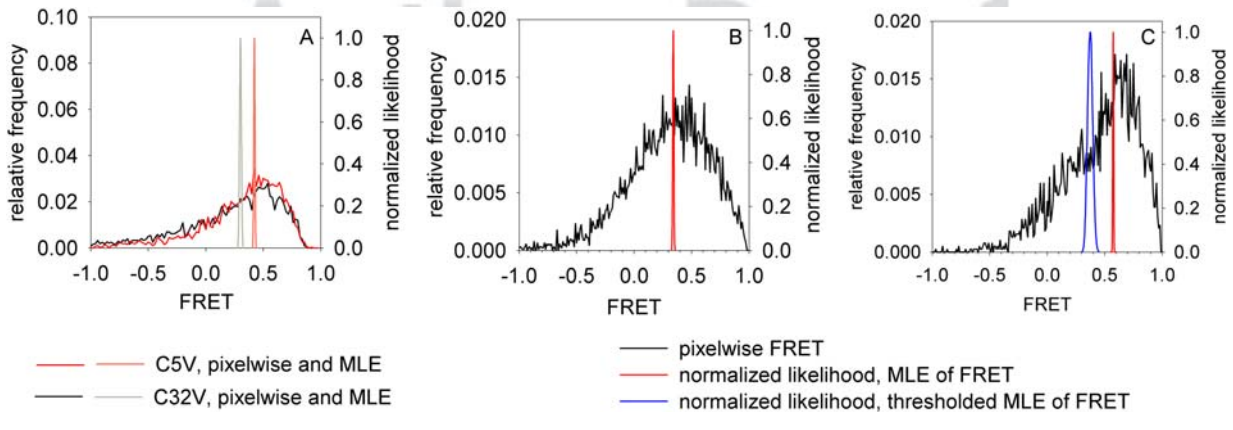

COLOR

Figure 4. Maximum likelihood estimation of FRET using Cerulean-Venus calibration constructs and antibody-labeled tissue samples. (**A**) Cells were transfected with a construct in which Cerulean and Venus were separated by a 5-amino acid (C5V) or a 32-amino acid linker (C32V). Images were captured in the donor, FRET and acceptor channels using a confocal microscope operating in the photon counting mode. FRET was determined on a pixel-by-pixel basis and the distribution of FRET values is displayed by the red and black lines. FRET was also calculated by MLE and the confidence interval of the determined FRET value is shown by the orange and gray lines. (**B,C**) Breast cancer tissue samples were labeled with AlexaFluor546-trastuzumab and AlexaFluor647-pertuzumab to measure intramolecular FRET between two non-overlapping epitopes of ErbB2. FRET between these epitopes was found to be 0.3 in cultured cells labeled with the same antibodies serving as a reference for the measurements with tissue samples. After determining the necessary spectroscopic constants FRET was calculated on a pixel-by-pixel basis and using MLE. The distribution of pixelwise FRET efficiencies and the confidence interval of MLE for an image without outlier pixels are shown in (B). An image in which outlier pixels seemed to be present (Supporting Information, Fig. S6) was analyzed. The distribution of pixelwise FRET values and the confidence interval of MLE and thresholded MLE of FRET are shown in (C).

ID: kandasamy.d Time: 13:54 I Path: N:/3b2/CYTO/Vol00000/140078/APPFile/JW-CYTO140078

J_ID: z3w Customer A_ID: CYTO22518 Cadmus Art: CYTO22518 Ed. Ref. No.: 14-065 Date: 28-July-14 Stage: Page: 11

pixelwise FRET values (Fig. 4C). These methods provided estimates which were closer to the peak above 0.5. On the other hand, thresholded MLE successfully eliminated 1,506 outlier pixels from the total of 2,365 analyzed pixels thereby providing an estimate corresponding to the peak under 0.5. This latter peak corresponds to non-outlier pixels, a conclusion reached by comparing it to the histogram in Figure 4B.

Conclusions

A. We have developed MLE of FRET efficiency and we have shown in simulations and experiments that it works in the presence of low photon numbers and outlier pixels, conditions known to be practically important in biology. Since only a single estimate is provided for a population of pixels, the ability to resolve spatial heterogeneity is lost. But analyzing regions of interest of ~100 pixels separately gives an opportunity for limited spatial resolution.
B. Only thresholded MLE performed well if outlier pixels were present in simulations and experiments, i.e. in datasets contaminated with noise other than photon counting statistics.
C. The distribution of pixelwise FRET efficiencies is meaningless at low intensities due to their large uncertainty. Therefore, resolving FRET efficiencies on a pixel-by-pixel basis is not possible under these experimental conditions.
D. The median of pixelwise FRET efficiencies turned out to be the most accurate estimate from among measures of central tendency. FRET calculations from summed intensities proved to be reliable in the absence of outlier pixels.
E. It is suggested that simulations with photon numbers similar to those recorded during experiments be carried out in order to gain insight into the skewness of pixelwise FRET efficiencies and to prevent false conclusions from being reached.
F. MLE of ratio parameters can be used for the estimation of spectroscopic overspill parameters required for the ratiometric determination of FRET both in the absence and presence of outlier pixels. In the latter case only thresholded MLE gave an accurate estimate for the overspill parameter.
G. In addition to instrumental factors the statistical nature of photon detection can also lead to an apparent intensity dependence of overspill parameters.

Literature Cited

1. Jares-Erijman EA, Jovin TM. FRET imaging. Nat Biotechnol 2003;21:1387–1395.
2. Nagy P, Vereb G, Damjanovich S, Mátyus L, Szöllősi J. Measuring FRET in flow cytometry and microscopy. In: Robinson JP, editor. Current Protocols in Cytometry. New York: John Wiley & Sons; 2006. pp 12.8.1–12.8.13.
3. Clegg RM. Förster resonance energy transfer – FRET what is it, why do it, and how it's done. In: Gadella TWJ, editor. Laboratory Techniques in Biochemistry and Molecular Biology. Volume 33. Elsevier; 2009. pp 1–57.
4. Beutler M, Makrogianneli K, Vermeij RJ, Keppler M, Ng T, Jovin TM, Heintzmann R. satFRET: Estimation of Förster resonance energy transfer by acceptor saturation. Eur Biophys J 2008;38:69–82.
5. Bastiaens PIH, Jovin TM. Fluorescence resonance energy transfer microscopy. In: Celis JE, editor. Cell Biology: A Laboratory Handbook. 2 ed. Volume 3. New York: Academic Press; 1998. pp 136–146.
6. Mekler VM. A photochemical technique to enhance sensitivity of detection of fluorescence resonance energy transfer. Photochem Photobiol 1994;59:615–620.
7. Bastiaens PI, Majoul IV, Verveer PJ, Soling HD, Jovin TM. Imaging the intracellular trafficking and state of the AB5 quaternary structure of cholera toxin. EMBO J 1996; 15:4246–4253.
8. Matkó J, Jenei A, Mátyus L, Ameloot M, Damjanovich S. Mapping of cell surface protein-patterns by combined fluorescence anisotropy and energy transfer measurements. J Photochem Photobiol B 1993;19:69–73.
9. Szabó Á, Horváth G, Szöllősi J, Nagy P. Quantitative characterization of the large-scale association of ErbB1 and ErbB2 by flow cytometric homo-FRET measurements. Biophys J 2008;95:2086–2096.
10. Bene L, Fulwyler MJ, Damjanovich S. Detection of receptor clustering by flow cytometric fluorescence anisotropy measurements. Cytometry 2000;40:292–306.
11. Nagy P, Vámosi G, Bodnár A, Lockett SJ, Szöllősi J. Intensity-based energy transfer measurements in digital imaging microscopy. Eur Biophys J 1998;27:377–389.
12. Zeug A, Woehler A, Neher E, Ponimaskin EG. Quantitative intensity-based FRET approaches–A comparative snapshot. Biophys J 2012;103:1821–1827.
13. Wlodarczyk J, Woehler A, Kobe F, Ponimaskin E, Zeug A, Neher E. Analysis of FRET-signals in the presence of free donors and acceptors. Biophys J 2007;94:986–1000.
14. Xia Z, Liu Y. Reliable and global measurement of fluorescence resonance energy transfer using fluorescence microscopes. Biophys J 2001;81:2395–2402.
15. Gordon GW, Berry G, Liang XH, Levine B, Herman B. Quantitative fluorescence resonance energy transfer measurements using fluorescence microscopy. Biophys J 1998;74:2702–2713.
16. Berney C, Danuser G. FRET or no FRET: A quantitative comparison. Biophys J 2003; 84:3992–4010.
17. Hoppe A, Christensen K, Swanson JA. Fluorescence resonance energy transfer-based stoichiometry in living cells. Biophys J 2002;83:3652–3664.
18. Roberti MJ, Giordano L, Jovin TM, Jares-Erijman EA. FRET Imaging by k(t) /k(f). Chemphyschem 2011;12:563–566.
19. Trón L, Szöllősi J, Damjanovich S, Helliwell SH, Arndt-Jovin DJ, Jovin TM. Flow cytometric measurement of fluorescence resonance energy transfer on cell surfaces. Quantitative evaluation of the transfer efficiency on a cell-by-cell basis. Biophys J 1984;45:939–946.
20. Nagy P, Bene L, Hyun WC, Vereb G, Braun M, Antz C, Paysan J, Damjanovich S, Park JW, Szöllősi J. Novel calibration method for flow cytometric fluorescence resonance energy transfer measurements between visible fluorescent proteins. Cytometry A 2005;67A:86–96.
21. Chen H, Puhl HL, 3rd, Koushik SV, Vogel SS, Ikeda SR. Measurement of FRET efficiency and ratio of donor to acceptor concentration in living cells. Biophys J 2006; 91:L39–L41.
22. Szalóki N, Doan-Xuan QM, Szöllősi J, Tóth K, Vámosi G, Bacsó Z. High throughput FRET analysis of protein-protein interactions by slide-based imaging laser scanning cytometry. Cytometry A 2013;83A:818–829.
23. Vámosi G, Baudendistel N, von der Lieth CW, Szalóki N, Mocsár G, Muller G, Brazda P, Waldeck W, Damjanovich S, Langowski J, et al. Conformation of the c-Fos/c-Jun complex in vivo: A combined FRET, FCCS, and MD-modeling study. Biophys J 2008;94:2859–2868.
24. Bene L, Ungvari T, Fedor R, Sasi Szabo L, Damjanovich L. Intensity correlation-based calibration of FRET. Biophys J 2013;105:2024–2035.
25. Chen Y, Periasamy A. Intensity range based quantitative FRET data analysis to localize protein molecules in live cell nuclei. J Fluoresc 2006;16:95–104.
26. Zal T, Gascoigne NR. Photobleaching-corrected FRET efficiency imaging of live cells. Biophys J 2004;86:3923–3939.
27. Clayton AH, Klonis N, Cody SH, Nice EC. Dual-channel photobleaching FRET microscopy for improved resolution of protein association states in living cells. Eur Biophys J 2005;34:82–90.
28. Gadella TW Jr., Jovin TM. Oligomerization of epidermal growth factor receptors on A431 cells studied by time-resolved fluorescence imaging microscopy. A stereochemical model for tyrosine kinase receptor activation. J Cell Biol 1995;129:1543–1558.
29. Hoppe AD, Shorte SL, Swanson JA, Heintzmann R. 3D-FRET reconstruction microscopy for analysis of dynamic molecular interactions in live cells. Biophys J 2008;95: 400–418.
30. Neher RA, Neher E. Applying spectral fingerprinting to the analysis of FRET images. Microsc Res Tech 2004;64:185–195.
31. Dalal RB, Digman MA, Horwitz AF, Vetri V, Gratton E. Determination of particle number and brightness using a laser scanning confocal microscope operating in the analog mode. Microsc Res Tech 2008;71:69–81.
32. Koushik SV, Chen H, Thaler C, Puhl HL 3rd, Vogel SS. Cerulean, Venus, and VenusY67C FRET reference standards. Biophys J 2006;91:L99–L101.
33. Nagy P, Bene L, Balázs M, Hyun WC, Lockett SJ, Chiang NY, Waldman F, Feuerstein BG, Damjanovich S, Szöllősi J. EGF-induced redistribution of erbB2 on breast tumor cells: Flow and image cytometric energy transfer measurements. Cytometry 1998;32: 120–131.
34. Roszik J, Sebestyen Z, Govers C, Guri Y, Szoor A, Palyi-Krekk Z, Vereb G, Nagy P, Szollosi J, Debets R. T-cell synapse formation depends on antigen recognition but not CD3 interaction: Studies with TCR:zeta, a candidate transgene for TCR gene therapy. Eur J Immunol 2011;41:1288–1297.
35. van Kempen GM, van Vliet LJ. Mean and variance of ratio estimators used in fluorescence ratio imaging. Cytometry 2000;39:300–305.
36. Webb DJ, Brown CM. Epi-fluorescence microscopy. Methods Mol Biol 2013;931:29–59.

ID: kandasamy.d Time: 13:54 I Path: N:/3b2/CYTO/Vol00000/140078/APPFile/JW-CYTO140078